Fractal model of superstructures on AgBr(111)

H. Hofmeister*
Solid State Physics Laboratory, Swiss Federal Institute of Technology, Hönggerberg, CH-8093 Zürich, Switzerland

S. Grosse and G. Gerth†
Max Planck Institute of Microstructure Physics, Weinberg 2, D-06120 Halle (Saale), Germany

H. Haefke
Institute of Physics, University of Basel, Klingelbergstrasse 82, CH-4056 Basel, Switzerland
(Received 2 April 1993)

It has recently been observed that thin film AgBr(111) may exhibit well-pronounced superstructures which are visualized by surface decoration, i.e., by deposition of a very small quantity of metal. Depending on the growth conditions of the AgBr films, these superstructures establish superlattices with ⟨110⟩ and ⟨321⟩ directions, respectively, of the AgBr lattice. They are thought to result from surface reconstruction of the otherwise highly polar surface. A fractal model of AgBr(111) superstructures is presented which for the first time, to our knowledge, enables us to assign the experimentally observed superlattices to surface configurations of proper dimensions and directions. By applying a simple procedure of covering the surface lattice sites so as to approach a half coverage, superstructures are formed which may stabilize the surface by coarsening on the atomic scale. The contribution of the subsurface space-charge layer, which is mainly due to mobile silver ion interstitials in a near surface region, as well as its possible interaction with neutral metal clusters formed at the surface during vapor deposition, are emphasized.

I. INTRODUCTION

Silver halides, central to photography, have retained their dominant role in photographic materials despite the impressive advances made recently in alternative technologies, particularly in electronic imaging. Their unique photographic properties are strongly affected by the surface structure. In modern high-speed photographic emulsions, containing octahedral grains or tabular microcrystals, the {111} surface is the prevailing face. For electrostatic reasons the {111} surfaces of crystals with NaCl-type lattices should undergo substantial reconstruction,[1] unless there is adsorption of impurities, because they consists of cations or anions only.

During more than two decades many attempts have been made to disclose te structure of AgBr(111),[1–10] Using electron microscopy, replica techniques and the surface decoration method, Hamilton and Brady[4] and more recently Haefke and Krohn,[11] have shown that these surfaces may exhibit well-pronounced superstructures. Small metal particles about 6 nm in size were found to be arranged in a two-dimensional array of threefold symmetry. In this way a superlattice with lattice distances varying from 5.9 to 8.3 nm (depending on the different film growth conditions applied) is formed. Hamilton and Brady[4] proposed a model for the surface ionic layer based on the charge compensation by a half-filled topmost layer of either silver or bromine ions. This specific model could not be confirmed by atomistic simulations.[9]

Up to now, however, no convincing atomistic models of such superstructures, as expected to be formed by surface reconstruction, have been given. Although recent studies employing scanning force microscopy (SFM) have also suggested the existence of a superstructure on {111} surfaces of AgBr thin films,[12] and tabular microcrystals,[13] the real-space configuration and the above-mentioned superstructures could not be revealed at an atomic scale.

In the present paper a fractal model based on a simple procedure of covering the lattice sites of AgBr(111) is introduced, enabling the construction of superstructures, the dimensions and directions of which agree fairly well with those of the experimentally observed superlattices. Despite the overall charge compensation achieved by applying this procedure, the surface configurations obtained may act as preferred sites of metal accommodation during vapor deposition because of locally uncompensated charges.

II. EXPERIMENTAL BACKGROUND AND RESULTS

Thin films of AgBr, which exhibit sufficiently large {111} faces at their surfaces, were grown under ultrahigh vacuum by vapor deposition on amorphous carbon layers, as well as mica at substrate temperatures between room temperature and 100 °C. The carbon substrates of about 20-nm thickness were prepared by vapor deposition on alkali halide cleavage faces at room temperature. The thickness of the AgBr films varied between 50 and 2000 nm. The decoration technique, applied to reveal the surface structure of the AgBr films, was performed by vapor deposition of gold of a nominal layer thickness of 0.2 nm. Fixation of the decoration patterns, i.e., the distribution of the gold particles grown on the AgBr surface, was

achieved by embedding the gold particles in a vapor-deposited Pt/C replica which could be separated from the AgBr films for electron microscopy inspection. For further experimental details, we refer to metal decoration experiments applied to {111} surfaces of AgBr films as presented by Haefke and co-workers.[11,12]

The electron micrographs obtained by conventional electron microscopy (JEM 100C operating at 100 kV) were digitized for further examination and treated by image processing routines (GATAN software "Digital Micrograph" and the NIH software "Image") to optimize the image contrast and to visualize in a Fourier-transform representation the space frequencies present in the decoration pattern as well as their angular distribution.

In spite of the different experimental conditions applied, at first sight the results obtained by depositing a very small amount of metal on the surface of AgBr films under appropriate conditions look quite similar: the {111} top faces of individual AgBr grains or islands are decorated by nearly equisized metal particles which are highly ordered along three directions so as to form a pattern, the smallest unit of which is an equilateral triangle. Going into more detail to find some particulars of the underlying superstructure, it becomes clear that there is not a single reconstructed structure of AgBr(111). This is because the geometrical and crystallographic details of the two-dimensional superlattice of metal particles are different in dependence on the growth conditions of the AgBr films.

Hamilton and Brady,[4] who first observed the decoration superlattice, report a superlattice distance of 7.0 nm with lattice directions parallel to ⟨321⟩ for the AgBr film that was grown at 100 °C to 100 nm thickness on a mica substrate. Haefke *et al.*[12] report a superlattice spacing of 5.9 nm with directions parallel to ⟨110⟩ of the AgBr film grown at room temperature to 500 nm thickness on a mica substrate. Haefke and Krohn[11] report a spacing of 8.3 nm with directions parallel to ⟨110⟩ of a discontinuous AgBr film that was grown at 300 °C to about 300 nm thickness on a LiF substrate.

On amorphous carbon, we observed a superlattice with a spacing of 5.6 nm and directions parallel to ⟨110⟩ of the AgBr film grown at 100 °C to 50 nm, and a superlattice with a spacing of 8.3 nm having directions parallel to ⟨321⟩ at about 2000 nm film thickness.[14] This is illustrated by Fig. 1, which shows the gold decorations obtained (a) at 50 nm thickness of the AgBr film, and (b) at 2000 nm thickness. The framed insets in the lower right, which are image-processed representations of the original micrographs, reveal more clearly the ordering of the gold particles. The spacings and directions of the decoration superlattices may be recognized quite distinctly from the Fourier transforms of the micrographs shown in the upper right. As may be noticed in Fig. 1(b) from the Fourier transform and from the arrow tripods, which mark the directions of the underlying AgBr lattice,[15] on the thicker AgBr film there are present two neighboring domains of the decoration superlattice rotated from each other by 38°.

In view of these results, we are not going to construct a single model that covers all the experimental details, but present different feasibilities of a fractal arrangement of surface ions to obtain a charge-compensating half coverage of AgBr(111). These will nevertheless lead inevitably to ordered top layers that exhibit fairly well arrays of dis-

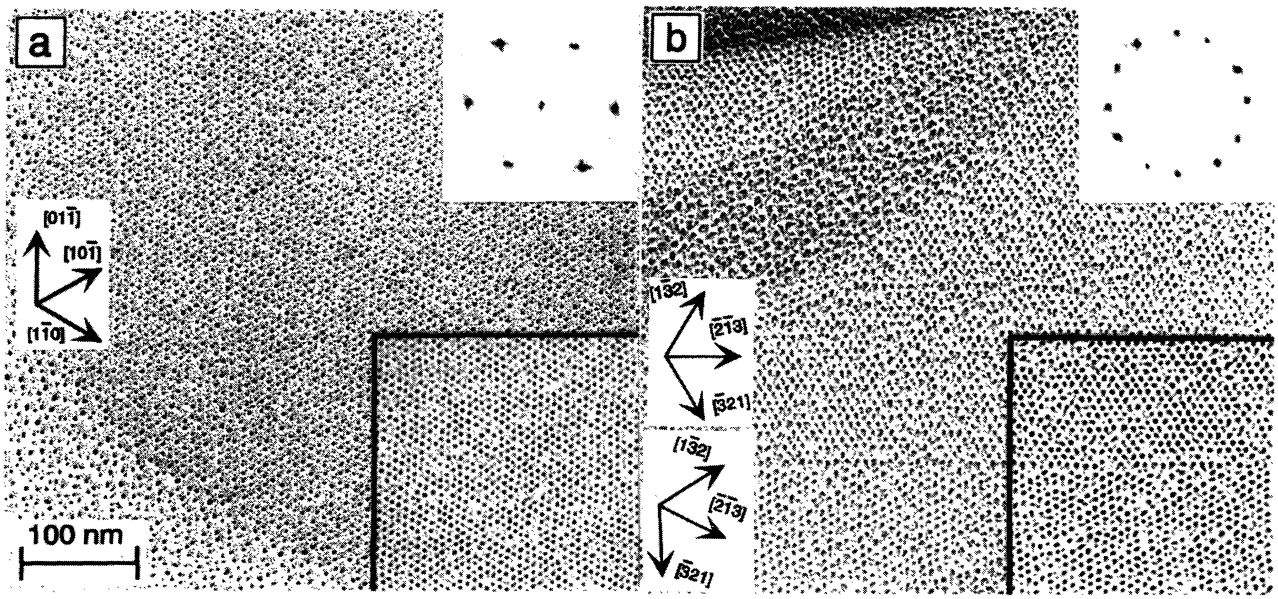

FIG. 1. Decoration patterns on {111} faces of AgBr formed by vapor deposition of gold at different thicknesses of the AgBr films: (a) at 50 nm with ⟨110⟩ directions of the superlattice: (b) at 2000 nm with ⟨321⟩ directions of the superlattice that is present in two neighboring domains rotated by 38°. The copies of the original micrographs are supplemented by image-processed real space (framed, lower right) and reciprocal space (upper right) representations that show more clearly the ordering of the gold particles. Outside of the {111} faces an irregular arrangement of the gold particles is found.

tinguished sites according to the decoration patterns observed.

III. A FRACTAL ARRANGEMENT OF THE HALF COVERAGE OF AgBr(111)

The simplest type of reconstruction of AgBr(111) that allows for charge compensation of the otherwise highly polar surface involves a half-layer of either bromine or silver ions as the topmost layer. Atomistic simulations using a criterion of minimum surface energy[9] have shown that half-layer surface models with the ions in their "normal" hollow-site positions are more stable than models with the ions placed in "bridge" site positions with respect to the second-layer ions. Taking this into account, two arrangements of ions on the surface layer have been proposed: the hexagonal arrangement[4] and the alternate row model.[9] A top view of both models is shown in Fig. 2, where the vacancies in the alternate row model (b) are marked by open circles. The hexagonal arrangement (a) does not use vacancy positions at normal lattice sites, but one third of the ions are in a twin position with respect to the second layer. It can easily be recognized that both models do not produce an arrangement of preferred sites whose dimensions are comparable to the metal particle superlattice. The same is valid for other models of Hamilton and Brady,[4] which indeed enable them to derive ⟨321⟩ directions but also involved the disadvantage of "bridge" sites.

In contrast to the equal distribution of ions and vacancies in a purely geometrical way, as proposed until now, we introduce a quite different way to achieve a half-covered surface layer. In order to meet the experimental findings, and also to prevent effectively the formation of dipole moments at the surface, we aim at arrangements of threefold symmetry. Since it is more favorable for energetic reasons, we take only normal lattice sites into consideration. A procedure for covering the lattice sites is used which involves the occupation by ions or vacancies as well as temporary nonoccupation. Special care is taken to avoid the formation of clusters of three nearest-neighbor ions that should cause repulsive interactions. Accordingly, in the following we present three different configurations satisfying these constraints, which are used as initial configurations to derive superlattices whose dimensions and directions agree with one of the experimentally observed superlattices.

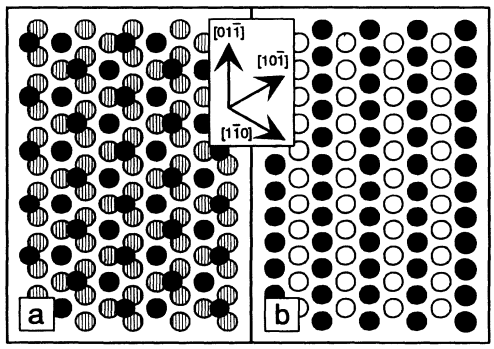

FIG. 2. Previous model arrangements of a half-coverage of the topmost layer of the AgBr surface: (a) hexagonal arrangement (Ref. 4), with the ions of the topmost layer marked by full circles and the ions of the complete underlying layer marked by hatched circles; (b) alternate row model (Ref. 9), with the ions marked by full circles and the vacancies marked by open circles.

A. Initial configuration with ⟨211⟩ directions

The initial configuration shown in Fig. 3(a) contains one-third of still unassigned lattice sites (shaded circles) which are surrounded symmetrically by ion positions (full circles) and vacancy positions (open circles). Each of these sites has the same neighbors. The still unassigned positions obtained by this first step of the covering procedure are connected by straight lines to visualize the so-formed two-dimensional superlattice that is enlarged by the factor $\sqrt{3}$ and rotated by 30° with respect to the original lattice. The rotation angle of 30° corresponds to that enclosed by the ⟨110⟩ and ⟨211⟩ directions of the {111} face. These still unassigned sites now have to be covered in such a way that not only is the half coverage approached, but also a superlattice of distinguished sites is obtained. This is achieved by means of the following rule of covering the lattice sites: alternating, one is occupied by an ion, another by a vacancy, and the third remains free to be occupied in a further step. In applying this rule, we again obtain a superlattice of still unassigned sites that is enlarged by $\sqrt{3}$ and rotated by 30° with respect to the foregoing one. The result of this second step is shown in Fig. 3(b), with the superlattice marked. By continuing in the way described, after n steps a superlattice is formed which is enlarged by $\sqrt{3^n}$ and rotated by $n\times 30°$ with respect to the original lattice.

The characteristic of the structure resulting from this procedure is the presence of branching nodes in the line that can be drawn to connect nearest-neighbor ion sites (or vacancy sites). This is illustrated by Fig. 3(c), which shows the branching structure of the ion sites after completing the fourth step of covering, with the numbers denoting the step at which the assignment took place. Three ion sites occupied in the first step (denoted by 1) always are linked by a node of first order that is an ion site occupied in the second step (denoted by 2). Three such branches of occupied sites are linked by a node of second order, i.e., a site occupied in the third step. Accordingly, all sites occupied in the nth step form nodes of $(n-1)$th order. As a consequence, after n steps a branching structure is produced at which the potential nodes of nth order are the still unassigned lattice sites representing the lattice points of the superlattice introduced above. The fractal nature[17,18] of this branching structure may be made clear by its self-similarity and scale invariance, i.e., changing the scale by a factor $\sqrt{3}$ keeps the structure unchanged.

The orientation and dimensions of the superlattice produced in the above-described manner are determined by the spacing and orientation relationships of the AgBr, lattice itself. With the lattice parameter of AgBr ($a=0.577$ nm), the distance of the rows of ion sites running in the ⟨110⟩ direction of the {111} surface equals

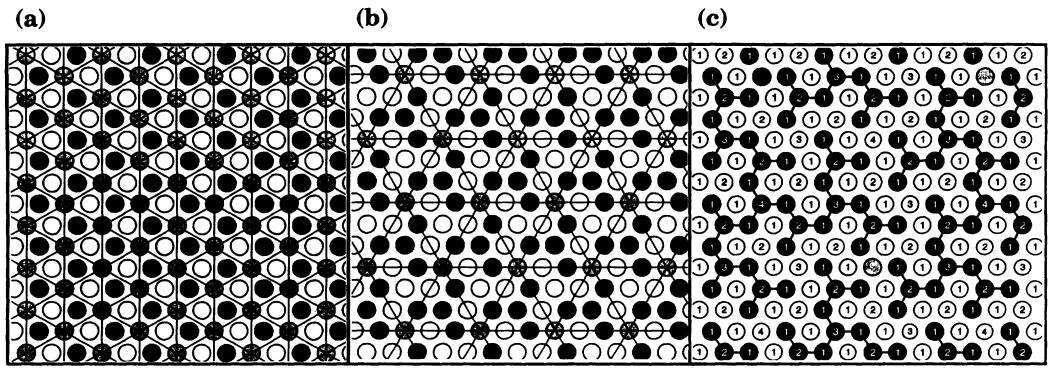

FIG. 3. Covering procedure for the ⟨211⟩ initial configuration. (a) First step, with ions (full circles), vacancies (open circles), and temporary nonoccupied sites (shaded circles). The superlattice (straight lines) formed by the still unassigned sites is enlarged by $\sqrt{3}$ and rotated by 30° with respect to the original lattice. (b) Second step. The superlattice (straight lines) formed by the still unassigned sites is enlarged by $\sqrt{3}$ and rotated by 30° with respect to the foregoing one. (c) Fourth step, with the branching structure of the ions marked by lines connecting the ion sites. The numbers denote the step at which the assignment took place.

0.354 nm. Consequently, with completing the sixth step the fractal arrangement established above represents a superlattice of still unassigned sites having a spacing of 9.55 nm and directions parallel to ⟨110⟩. With this there remains a deficit in the half coverage by ions of 0.069% that corresponds to 5.42×10^{11} ions per cm^2.

B. Initial configuration with ⟨110⟩ directions

With the prerequisite of threefold symmetry, a second initial configuration that makes use of normal lattice sites only is shown in Fig. 4(a). It contains one fourth of still not assigned lattice sites (shaded circles) which are surrounded symmetrically by ion positions (full circles) and vacancy positions (open circles). Besides rotations by 60°, each second of these sites has the same neighbors. The superlattice of still unassigned positions (marked by straight lines) obtained by this first step of the procedure is enlarged by the factor $\sqrt{4}$ with respect to the original lattice. Covering these sites by the rule applied in Sec. III A will result in a superlattice of still unassigned sites that is enlarged by $\sqrt{3}$ and rotated by 30° with respect to the foregoing one. The result of this second step is shown in Fig. 4(b) with the superlattice marked by straight lines. By continuing in the well-tried way, after n steps a superlattice is formed that is enlarged by $\sqrt{4}\times\sqrt{3^{(n-1)}}$ and rotated by $(n-1)\times30°$ with respect to the original lattice.

As may be seen from Fig. 4(c) that corresponds to the situation after completing the fourth-step of covering, also with this initial configuration a branching structure is obtained by applying the covering rule. By comparison with Fig. 3(c) it comes clear that now the branching nodes of first order (denoted by 2) do not connect single ions but groups of three ions that themselves resemble the basic motif of the branching. Here the fifth step of the covering procedure leads to fractal arrangement that represents a superlattice of still unassigned sites having a spacing of 6.36 nm and directions parallel to ⟨110⟩. A deficit in the half coverage by ions of 0.15% remains with this that corresponds to 1.22×10^{12} ions per cm^2.

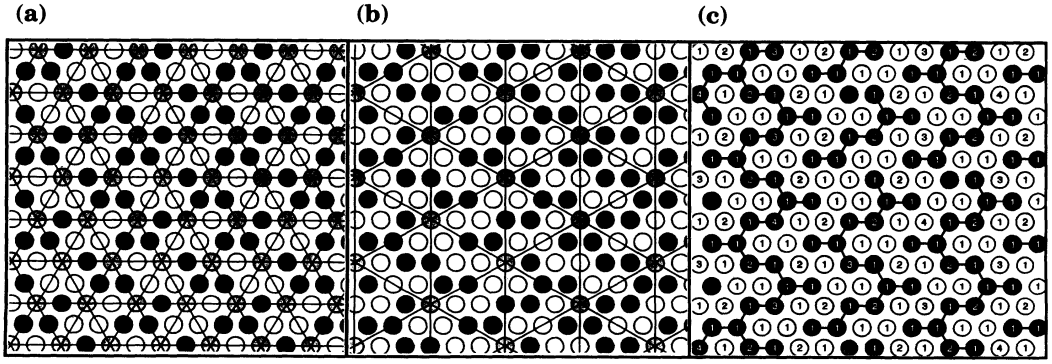

FIG. 4. Covering procedure for the ⟨110⟩ initial configuration. (a) First step, with ions (full circles), vacancies (open circles), and temporary nonoccupied sites (shaded circles). The superlattice (straight lines) formed by the still unassigned sites is enlarged by $\sqrt{4}$ with respect to the original lattice. (b) Second step. The superlattice (straight lines) formed by the still unassigned sites is enlarged by $\sqrt{3}$ and rotated by 30° with respect to the foregoing one. (c) Fourth step, with the branching structure of the ions marked by lines connecting the ion sites. The numbers denote the step at which the assignment took place.

C. Initial configuration with ⟨321⟩ directions

A third initial configuration, established according to the constraints described above, is shown in Fig. 5(a). It contains one seventh of still unassigned lattice sites (shaded circles) which are surrounded symmetrically by ion positions (full circles) and vacancy positions (open circles). Besides rotations by 60°, each of these sites has the same neighbors. The configuration resulting from this first step exhibits a two-dimensional superlattice of still unassigned sites (marked by straight lines) which is enlarged by the factor $\sqrt{7}$ and rotated by 19.1° with respect to the original lattice. The rotation angle of 19.1° corresponds to that enclosed by the ⟨110⟩ and ⟨321⟩ directions of the {111} face. Since there are two possibilities of performing this rotation (clockwise or anticlockwise) to arrive at one of the two ⟨321⟩ directions that always run symmetrically to a ⟨110⟩ direction, there are two equivalent initial configurations possible which are rotated to each other by 38.2°.

Now the still unassigned sites have to be covered by means of the rule already applied in Secs. III A and III B. This will result in a superlattice of still unassigned sites that is enlarged by $\sqrt{3}$ and rotated by 30° with respect to the foregoing one. The result of this second step, with the superlattice marked, is shown in Fig. 5(b). By continuing in the well-tried way, after n steps a superlattice is formed which is enlarged by $\sqrt{7}\times\sqrt{3^{(n-1)}}$ and rotated by $19.1°+(n-1)\times 30°$ with respect to the original lattice.

In fact, this procedure also results in a branching structure that is shown in Fig. 5(c) for the ion sites after completing the fourth step of covering. As was the case with the branching structure described in Sec. III B, here also the branching nodes of first order (denoted by 2) do not connect single ions but groups of three ions which themselves resemble the basic motif of the branching. Completing the fifth step of covering the fractal arrangement established in this manner represents a superlattice of still unassigned sites having a spacing of 8.42 nm and directions parallel to ⟨321⟩. With this there remains a deficit in the half coverage by ions of 0.088% that corresponds to 6.97×10^{11} ions per cm^2.

IV. DISCUSSION

The representation of the fractal arrangement of ions and vacancies as a branching structure is quite appropriate to explain the formation of regular arrays of metal particles by vapor deposition. Regarding the branching structure as a graph of diffusion paths, the branching nodes are places of enhanced meeting probability for diffusing atoms, where the higher the order of the node the more enhanced this probability. It is important to note that the branching nodes effectively are centers of locally uncompensated charges. The distances at which these charges are compensated increase with the order of the nodes. By model calculations it may be shown that the stability of ions in such node positions decreases with the increasing order of the node.[19] This peculiarity enables the branching nodes of higher order to act as preferred sites of nucleation of neutral metal clusters in the process of vapor deposition. Actually, the uncompensated charges at the emergence points of step dislocation in sodium chloride cleavage faces have been proven to act exactly in this manner, so as to enable a decoration of such points by metal particles.[20]

Polar faces of ionic crystals may be stabilized by superstructures based on the nonoccupation of certain surface positions,[3,4,9,21,22] whereby dipole moments perpendicular to the surface may be removed and repulsive interactions between equally charged surface ions may be reduced, respectively. Up to now, only models of periodic incomplete filling of surface sites have been reported to interpret experimental findings,[4] or to estimate the specific surface energy of such structures.[9] From direct energy calculations, clearly a tendency toward a coarsening on the atomic scale is to be expected for the {111} face of NaCl-type crystals.[23]

Instead of viewing the NaCl lattice as a fcc bravais lattice with a dipolar basis molecule, recent surface energy calculations make use of the possibility to view it as a simple cubic lattice with an octopolar $(NaCl)_4$ basis,[24,25] as is shown in Fig. 6(a). Here the differently charged ions are marked by filled and hatched circles. The numbers 1, 2, and 3 denote the (001), (100), and (010) facets which form the unit cell. If viewing the crystal, which is re-

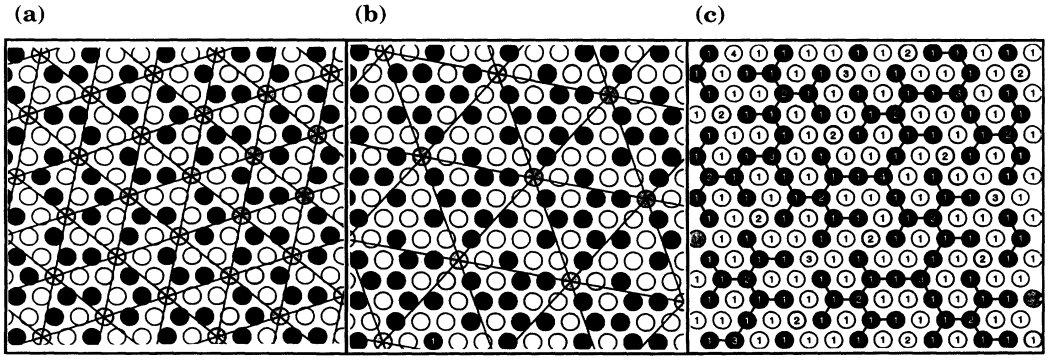

FIG. 5. Covering procedure for the ⟨321⟩ initial configuration. (a) First step, with ions (full circles), vacancies (open circles), and temporary nonoccupied sites (shaded circles). The superlattice (straight lines) formed by the still unassigned sites is enlarged by $\sqrt{7}$ and rotated by 19.1° with respect to the original lattice. (b) Second step. The superlattice (straight lines) formed by the still unassigned sites is enlarged by $\sqrt{3}$ and rotated by 30° with respect to the foregoing one. (c) Fourth step, with the branching structure of the ions marked by lines connecting the ion sites. The numbers denote the step at which the assignment took place.

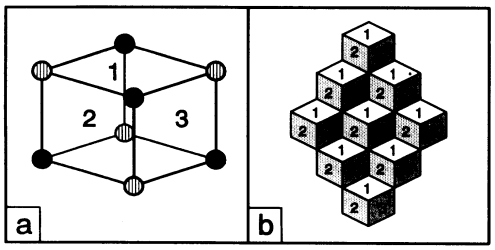

FIG. 6. Simple cubic representation of the NaCl-type lattice: (a) the octopolar basis, where full circles and hatched circles mark the differently charged ions and the numbers 1–3 denote the cube facets; (b) tiling of the plane triangle lattice in the case of the ideal {111} face with the cube facets of the octopolar unit cell.

garded now as a set of stacked octopolar cubes along ⟨111⟩, a periodic "diamond" tiling of the plane triangular lattice in case of the ideal {111} surface is obtained,[26] as is sketched in Fig. 6(b). Where two facets of different orientation (denoted by 1–3) meet, an edge is formed, and where three or more edges meet, a corner is formed. Accordingly, the ideal planar {111} face consists of a periodic arrangement of corners stepping forward and backward, with respect to the plane of the figure, which are formed by the meeting of three edges, and of corners in the medium position which are formed by the meeting of six edges, respectively. The octopolar representation opens a way of assigning energies to complex surface configurations that involve only a local surface structure such as the exposed cube facets, edges, and corners, respectively.

It is obvious to use the octopolar representation in order to view the fractal arrangements derived for the half covered AgBr(111). The result of this transformation applied to the configurations with superlattice directions parallel to ⟨110⟩ and ⟨321⟩ as represented by the branching structures shown in Figs. 3(c), 4(c), and 5(c), respectively, is shown in Figs. 7(a), 7(b), and 7(c). These drawings reproduce only selections, turned by 180° of the corresponding tilings. It may be recognized that in all cases aperiodic tilings are obtained which exhibit distinct microscopic configurations. In contrast to the ideal {111} face, here agglomerations of cube facets of equal orientation occur, which enables to consider the surface structure as coarsened on the atomic scale. While in Figs. 7(a) and 7(b) there are agglomerations of two, three, and four equioriented facets, Fig. 7(c) also exhibits agglomerations of five equal facets. By these specifications of the surface configurations derived to interpret the decoration superlattice, we intend to evaluate the electrostatic part of the surface energy in order to find out to which extent the configurations are energetically favored.

Actually, a direct proof that the structures obtained by the model considerations given above are energetically favorable still is missing. This is supported indirectly by the fact that these configurations are structurally reasonable in terms of the coarsening of the {111} face on the atomic scale, and because they are experimentally observable, at least by means of their macroscopic dimensions and orientations. As to the macroscopic dimensions, a comparison of the spacings experimentally observed from the decoration superlattice and those obtained from model considerations shows certain discrepancies. These shall be discussed first with the most recent measurements, i.e., those of AgBr on amorphous carbon, which resulted in superlattice spacings of 5.6 and 8.3 nm for the two different directions. In this connection it must be pointed out that, first, the measurements are not performed at the surfaces themselves, but at replicas containing "markers" of the distinguished sites in the form of metal particles, whereby a certain shrinkage or swelling of the replica because of the preparation processes can not be excluded. Second, the markers are not located directly at the site itself, but may be disarranged because of growth processes, which makes a statistical contribution to the result of the measurements. Third, there is a measuring error, common to the examination of electron micrographs because of uncertainties relating to the magnification scale, that is

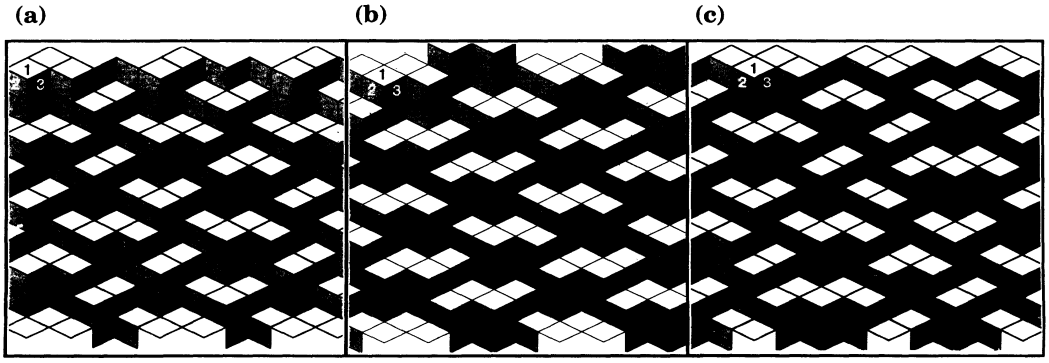

FIG. 7. Tiling with octopolar cube facets of the fractal arrangement, (a) derived from the ⟨211⟩ initial configuration after completing the fourth step of the covering procedure [selection of Fig. 3(c) turned by 180°]; (b) derived from the ⟨110⟩ initial configuration after completing the fourth step of the covering procedure [selection of Fig. 4(c) turned by 180°]; (c) derived from the ⟨321⟩ initial configuration after completing the fourth step of the covering procedure [selection of Fig. 5(c) turned by 180°].

usually in the order of 3–5 %. Therefore, qualifying by error sums the figures of the superlattice spacings mentioned at the beginning, one has to compare 5.6±0.6 nm of the ⟨110⟩ decoration superlattice with 6.36 nm of the corresponding model structure, and 8.3±0.8 nm of the ⟨321⟩ decoration superlattice with 8.42 nm of the corresponding model structure. In this connection, indeed we can speak of a fairly good agreement. This also applies to the 5.9-nm superlattice spacing with ⟨110⟩ directions reported by Haefke *et al.*[12]

Considering in this context the results of Hamilton and Brady,[4] who reported a 7.0-nm superlattice spacing with ⟨321⟩ directions (to be compared with 8.42 nm), and those of Haefke and Kron[11] who reported 8.3-nm superlattice spacing with ⟨110⟩ directions (to be compared with 9.55 nm), we are inclined to attribute these discrepancies to exceptionally large measuring errors, preparation-dependent large-scale distortions, or a combination of both, respectively. In spite of such deviations, it should be emphasized here that the model clearly allows us to predict the presence of two domains rotated to each other by 38.2° in the case of the superlattice with directions parallel to ⟨321⟩, as was experimentally observed[4,14] and is shown in Fig. 1(b) of this paper. This is simply a consequence of two equivalent initial configurations, as mentioned in Sec. III C. An explanation of the occurrence of the ⟨321⟩ superlattice in addition to the ⟨110⟩ superlattice at an increased AgBr film thickness must be addressed to further experiments and model considerations.

Nevertheless, the question arises of what may be the reason for the development of such starting configurations, and what is the driving force to form a fractal arrangement of half coverage from it. Although the configurations themselves and the single steps involved are reasonable since they obey the requirements of both, avoiding far-reaching dipole moments at the surface and a global charge compensation, at the moment we only can speculate on these inquiries. The speculations may be directed to two different points: one is the role of the subsurface space-charge layer experimentally evidenced for AgBr(111),[2,9] and the other is the role of neutral metal atoms arriving from the vapor phase in the process of decoration.

The presence of a subsurface space-charge layer, consisting of an excess of silver ions on interstitial sites, and a deficiency of silver ion vacancies, which are balanced by an excess of silver ion vacancies at the very surface, gives support to the idea that the half-covered topmost layer of AgBr(111) should contain silver ions.[4,9] This is suggested also by the interpretation of surface-extended x-ray-absorption fine structure (SEXAFS) data.[10] Since the subsurface space-charge layer is detected to contain about 1×10^{13} unit charges per cm^2,[2,4,27] it is assumed that a corresponding part of the silver ions of the topmost layer is removed into the subsurface space-charge region.[4] The silver ions remaining at the surface then may take up favorable equilibrium positions. It is quite obvious to apply these considerations to the configurations obtained by our covering procedure. In this connection, it should be pointed out that this procedure does not automatically lead to a complete half coverage of the topmost layer, but a deficiency is left which is slightly below the order of the silver ion concentration needed to built up the space-charge layer.

This astonishing agreement gives strong support to the overall correctness of the model procedures applied. As to the details of these procedures, however, we must be aware that the steps involved, although reasonable, represent an artificial process, the true atomistic description of which remains unclear. Indications of a possible contribution to these procedures from neutral metal atoms, arriving from the vapor phase and nucleating to form clusters, come from scanning tunneling microscopy (STM) studies at the graphite (0001) surface. In the neighborhood of very small metal particles, obtained by vapor deposition on freshly cleaved graphite surfaces, Xhie and co-workers[28,29] observed a number of superstructures that are ascribed to periodic charge-density modulations due to perturbations of the graphite surface charge density by the metal particles. A few of these superstructures imaged by STM are quite similar to parts of the branching structures formed in the course of our model procedures. What one may conclude from this, with respect to the superlattices formed on AgBr(111), is no less than a certain sensitivity of the subsurface space-charge layer, which is due mainly to mobile silver ion interstitials, to the formation of neutral metal clusters during vapor deposition for decoration purposes.

Since the computer simulations of surface structures presented up to now for AgBr{111} (Ref. 9) hardly allow us to differentiate between various models because of very slight differences in the surface energies estimated, it cannot be excluded at present that the interaction between the subsurface space-charge layer and the just-forming metal clusters may, from the very beginning of the deposition process, play an important role in the formation of the configurations which finally are observed as decoration superlattices. To clarify more accurately these peculiarities of the reconstruction of AgBr(111), a comprehensive study by STM and SFM of carefully prepared and treated AgBr surfaces is now in progress.

V. CONCLUSIONS

We have introduced a method of constructing superstructures of AgBr(111) which fulfill the requirements of overall charge compensation, and exhibit arrays of distinguished surface sites, the characteristics of which, spacings and directions, agree quite well with those of the experimentally observed superlattices of metal particles. These distinguished sites, obtained by a fractal arrangement of ions and vacancies in the topmost layer, may act as preferred sites of metal accommodation during vapor deposition, since they carry locally uncompensated charges. By representing these surface configurations in view of a set of stacked octopolar cubes, distinct coarsenings on the atomic scale result which gives support to the idea that the superstructures effectively contribute to a surface stabilization. Because of a lack of clear experimental evidence as well as substantiated calculations of

the surface energy, the contribution of the subsurface space-charge layer as well as its possible interaction with neutral metal clusters formed at the surface during vapor deposition are only emphasized in a more speculative manner. A final treatment must be addressed to further experimental studies as well as calculations.

ACKNOWLEDGMENTS

The first author wishes to express his gratitude to Professor H.-U. Nissen for his kind hospitality and for exciting discussions during the stay at his laboratory in Zürich.

---

*Permanent address (to which correspondence should be addressed): Max Planck Institute of Microstructure Physics, Weinberg 2, D-06120 Halle (Saale), Germany.

†Present address: Institute of Physics, University of Basel, Klingelbergstrasse 82, CH-4056 Basel, Switzerland.

[1]P. W. Tasker, J. Phys. C **12**, 4977 (1979).

[2]V. I. Saunders, R. W. Tyler, and W. West, J. Photogr. Sci. Eng. **12**, 90 (1968).

[3]F. Trautweiler, L. E. Brady, J. W. Castle, and J. F. Hamilton, in *The Structure and Chemistry of Solid Surfaces,* edited by G. A. Somorjai (Wiley, New York, 1969), p. 83-1.

[4]J. F. Hamilton and L. E. Brady, Surf. Sci. **23**, 389 (1970).

[5]R. C. Baetzold and J. F. Hamilton, Surf. Sci. **33**, 461 (1972).

[6]Y. T. Tan, J. Appl. Phys. **46**, 469 (1975).

[7]C. R. Berry, J. Photogr. Sci. Eng. **20**, 29 (1976).

[8]H. Hoyen, in *The Physics of the Latent Image Formation in Silver Halides,* edited by A. Baldereschi *et al.* (World Scientific, Singapore, 1984), p. 151.

[9]R. C. Baetzold, Y. T. Tan, and P. W. Tasker, Surf. Sci. **195**, 579 (1988).

[10]P. Tangyunyong, T. N. Rhodin, Y. T. Tan, and K. Lushington, Surf. Sci. **255**, 259 (1991).

[11]H. Haefke and M. Krohn, Surf. Sci. **261**, L39 (1992).

[12]H. Haefke, E. Meyer, L. Howald, U. Schwarz, G. Gerth, and M. Krohn, Ultramicroscopy **42-44**, 290 (1992).

[13]U. D. Schwartz, J. Bohonek, H. Haefke, T. A. Jung, E. Meyer, R. Steinger, and H.-J. Gütherodt, Helv. Phys. Acta **65**, 874 (1992).

[14]S. Grosse and G. Gerth (unpublished).

[15]The directions of the underlying AgBr lattice are identified (see also Refs. 11 and 12 for this) by taking advantage of the epitaxy effect (see Ref. 16) from an electron-diffraction analysis of the areas concerned.

[16]H. Haefke, H. Hofmeister, and M. Krohn, J. Inform. Record. Mater. **15**, 123 (1987).

[17]B. B. Mandelbrot, in *Fractal Geometry of Nature* (Freemann, New York, 1983), pp. 151 and 326.

[18]N. E. Cusak, in *The Physics of Structurally Disordered Matter,* edited by D. F. Brewer (Hilger, Bristol, 1987), p. 47.

[19]E. Müller (private communication).

[20]H. Bethge, R. Scholz, and V. Schmidt, Discuss. Faraday Soc. **38**, 79 (1964).

[21]R. W. Nosker, P. Mark, and J. D. Levine, Surf. Sci. **19**, 291 (1970).

[22]W. W. Lee and S. Choi, J. Chem. Phys. **72**, 6164 (1980).

[23]E. Müller, Z. Phys. Chem. **269**, 113 (1988).

[24]R. Lacmann, Colloq. Int. CNRS **152**, 195 (1965).

[25]D. Wolf, Phys. Rev. Lett. **68**, 3315 (1992).

[26]A.-C. Shi and M. Wortis, Phys. Rev. B **37**, 7793 (1988).

[27]J. F. Hamilton, Adv. Phys. **37**, 359 (1988).

[28]J. Xhie, K. Sattler, U. Müller, N. Venkateswaran, and G. Raina, Phys. Rev. B **43**, 8917 (1991).

[29]J. Xhie, K. Sattler, M. Ge, and N. Venkateswaran, in *Physics and Chemistry of Finite Systems: From Clusters to Crystals,* edited by P. Jena *et al.* (Kluwer, Dordrecht, 1992), Vol. 11, p. 1159.

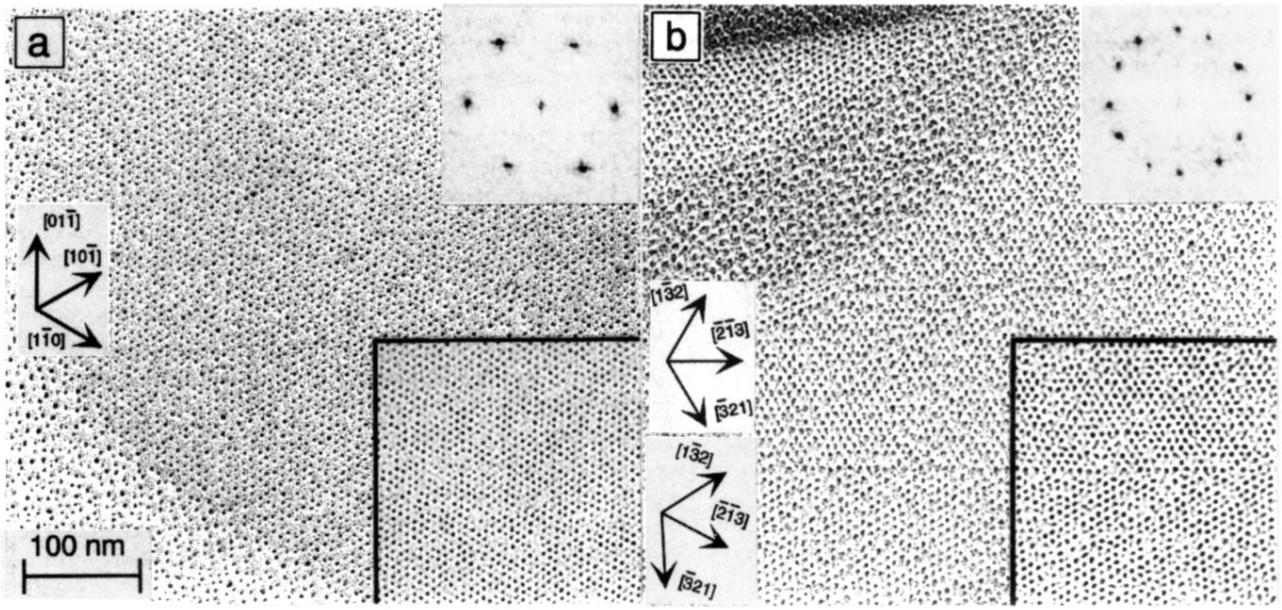

FIG. 1. Decoration patterns on {111} faces of AgBr formed by vapor deposition of gold at different thicknesses of the AgBr films: (a) at 50 nm with ⟨110⟩ directions of the superlattice: (b) at 2000 nm with ⟨321⟩ directions of the superlattice that is present in two neighboring domains rotated by 38°. The copies of the original micrographs are supplemented by image-processed real space (framed, lower right) and reciprocal space (upper right) representations that show more clearly the ordering of the gold particles. Outside of the {111} faces an irregular arrangement of the gold particles is found.

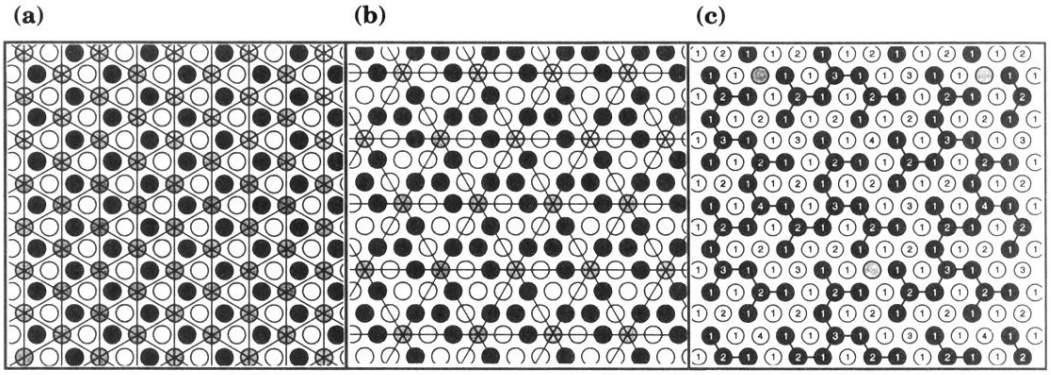

FIG. 3. Covering procedure for the ⟨211⟩ initial configuration. (a) First step, with ions (full circles), vacancies (open circles), and temporary nonoccupied sites (shaded circles). The superlattice (straight lines) formed by the still unassigned sites is enlarged by $\sqrt{3}$ and rotated by 30° with respect to the original lattice. (b) Second step. The superlattice (straight lines) formed by the still unassigned sites is enlarged by $\sqrt{3}$ and rotated by 30° with respect to the foregoing one. (c) Fourth step, with the branching structure of the ions marked by lines connecting the ion sites. The numbers denote the step at which the assignment took place.

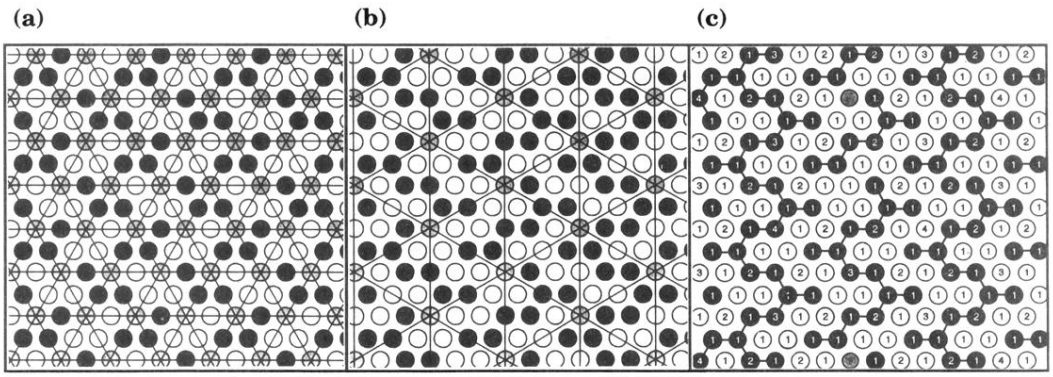

FIG. 4. Covering procedure for the ⟨110⟩ initial configuration. (a) First step, with ions (full circles), vacancies (open circles), and temporary nonoccupied sites (shaded circles). The superlattice (straight lines) formed by the still unassigned sites is enlarged by $\sqrt{4}$ with respect to the original lattice. (b) Second step. The superlattice (straight lines) formed by the still unassigned sites is enlarged by $\sqrt{3}$ and rotated by 30° with respect to the foregoing one. (c) Fourth step, with the branching structure of the ions marked by lines connecting the ion sites. The numbers denote the step at which the assignment took place.

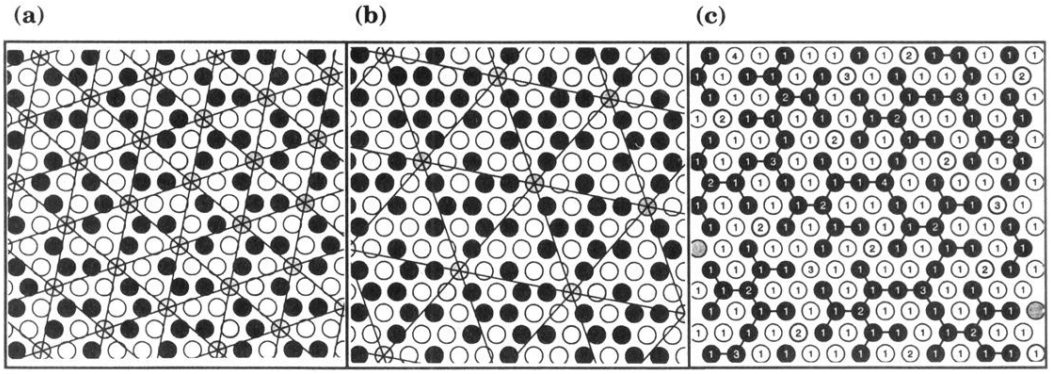

FIG. 5. Covering procedure for the $\langle 321 \rangle$ initial configuration. (a) First step, with ions (full circles), vacancies (open circles), and temporary nonoccupied sites (shaded circles). The superlattice (straight lines) formed by the still unassigned sites is enlarged by $\sqrt{7}$ and rotated by 19.1° with respect to the original lattice. (b) Second step. The superlattice (straight lines) formed by the still unassigned sites is enlarged by $\sqrt{3}$ and rotated by 30° with respect to the foregoing one. (c) Fourth step, with the branching structure of the ions marked by lines connecting the ion sites. The numbers denote the step at which the assignment took place.

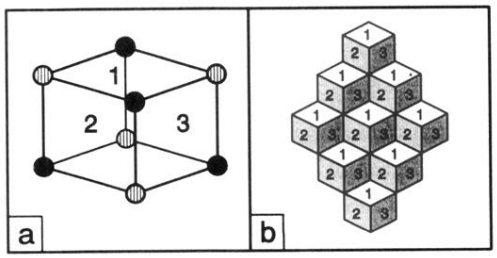

FIG. 6. Simple cubic representation of the NaCl-type lattice: (a) the octopolar basis, where full circles and hatched circles mark the differently charged ions and the numbers 1–3 denote the cube facets; (b) tiling of the plane triangle lattice in the case of the ideal $\{111\}$ face with the cube facets of the octopolar unit cell.

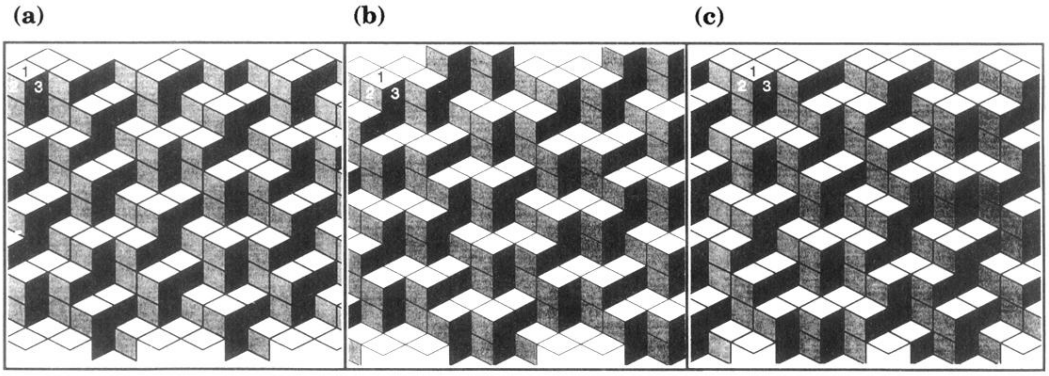

FIG. 7. Tiling with octopolar cube facets of the fractal arrangement, (a) derived from the ⟨211⟩ initial configuration after completing the fourth step of the covering procedure [selection of Fig. 3(c) turned by 180°]; (b) derived from the ⟨110⟩ initial configuration after completing the fourth step of the covering procedure [selection of Fig. 4(c) turned by 180°]; (c) derived from the ⟨321⟩ initial configuration after completing the fourth step of the covering procedure [selection of Fig. 5(c) turned by 180°].